



# Observation of the Hanbury Brown-Twiss effect with ultracold molecules

Jason S. Rosenberg<sup>⊕1,3</sup>, Lysander Christakis<sup>1,3</sup>, Elmer Guardado-Sanchez<sup>1,2</sup>, Zoe Z. Yan<sup>⊕1</sup> and Waseem S. Bakr<sup>⊕1⊠</sup>

Measuring the statistical correlations of individual quantum objects provides an excellent way to study complex quantum systems. Ultracold molecules represent a powerful platform for quantum simulation and quantum computation due to their rich and controllable internal degrees of freedom. However, the detection of correlations between single molecules in an ultracold gas has yet to be demonstrated. Here we observe the Hanbury Brown-Twiss effect—the emergence of bunching correlations of indistinguishable particles collected by separate detectors—in a gas of bosonic <sup>23</sup>Na<sup>87</sup>Rb Feshbach molecules, enabled by the realization of a molecular quantum gas microscope. We detect the characteristic bunching correlations in the density fluctuations of a two-dimensional molecular gas released from and subsequently recaptured in an optical lattice. The quantum gas microscope allows us to extract the positions of individual molecules with single-site resolution. As a result, we obtain a two-molecule interference pattern with high visibility. Although these measured correlations purely arise from the quantum statistics of the molecules, the demonstrated imaging capabilities open the way for site-resolved studies of interacting molecular gases in optical lattices.

In a landmark series of experiments in the 1950s, Hanbury Brown and Twiss (HBT) demonstrated the bunching correlations of photons from chaotic sources of light arriving at two detectors<sup>3,4</sup>. Their interferometry technique had practical applications in measuring the angular diameter of stars and led Glauber to develop a theory of quantum coherence, laying the foundation for the field of quantum optics<sup>5</sup>. In contrast to conventional interference observed, for example, in Young's double-slit experiment, the HBT effect results from the interference of two-particle rather than single-particle amplitudes—regardless of whether those 'particles' are photons, quasiparticles or matter. HBT interferometry has become a workhorse in high-energy and nuclear physics to probe the space–time geometry of collision volumes<sup>6</sup>. The effect has also been demonstrated with electrons<sup>7,8</sup>, neutrons<sup>9</sup> and phonons<sup>10,11</sup>.

In the field of ultracold quantum gases, the exquisite control afforded by modern experimental techniques has stimulated a wealth of intensity interferometry measurements in atomic systems, both bosonic<sup>12–21</sup> and fermionic<sup>16,22,23</sup>. Molecular gases are now routinely prepared in the ultracold regime where quantum effects play an important role<sup>1,24,25</sup>, often by leveraging the powerful approach of associating two ultracold atoms into a single molecule<sup>24</sup>. These molecules represent the most complex objects for which full control over all the motional and internal degrees of freedom has been demonstrated. Heteronuclear molecules are of particular interest

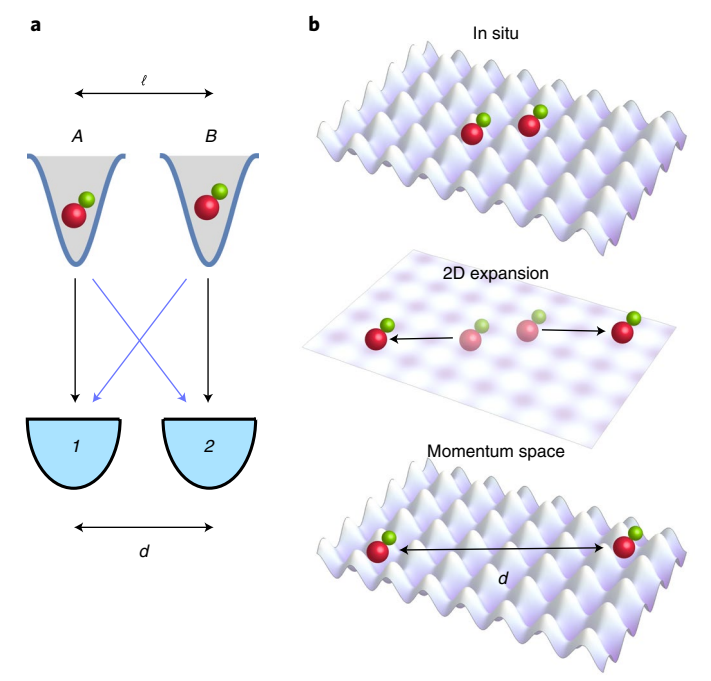


**Fig. 1 | HBT interference of heteronuclear bosonic molecules. a,** Molecules released from the lattice sites separated by distance  $\ell$  are detected after a TOF at variable separation d. The amplitudes associated with the shown two-particle trajectories (black and blue) interfere, leading to a joint detection probability that depends on d. **b**, The experiment in **a** is performed with molecules in an optical lattice. Multiple molecules are trapped in a 2D optical lattice (top). The 2D lattice is abruptly shut off, allowing the molecules to freely expand in the plane (middle). This expansion provides a transformation from position space to momentum space. An additional vertical lattice (not pictured) is left on to levitate the molecules against gravity. The molecules are recaptured in the 2D lattice after TOF, and their positions are measured with a quantum gas microscope (bottom).

because they can have a large, tunable electric dipole moment in their ground state. Recent experiments have detected individual heteronuclear molecules in small arrays<sup>26–28</sup> and have studied strongly interacting many-body systems in optical lattices<sup>29</sup>.

As two-particle correlations form a crucial experimental probe for interacting many-body systems comprising polar molecules,

<sup>&</sup>lt;sup>1</sup>Department of Physics, Princeton University, Princeton, NJ, USA. <sup>2</sup>Present address: Department of Physics, Harvard University, Cambridge, MA, USA. <sup>3</sup>These authors contributed equally: Jason S. Rosenberg, Lysander Christakis. <sup>™</sup>e-mail: wbakr@princeton.edu

NATURE PHYSICS LETTERS

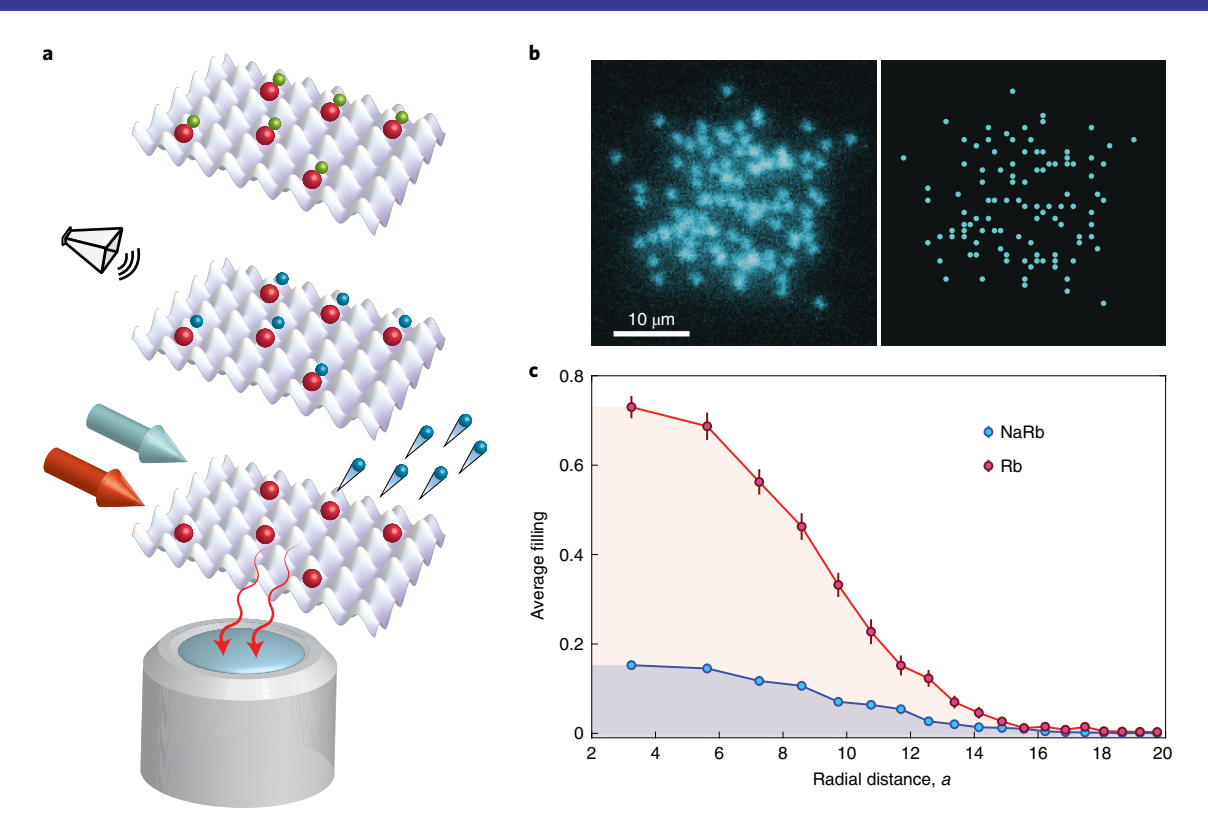


**Fig. 2 | Microscopy of molecules in an optical lattice. a**, Three-step process for detecting the molecules. An array of NaRb molecules is prepared in a lattice (top). A microwave Landau–Zener sweep flips the Na atoms from the |1,1) to |2,2) state, breaking apart the molecules into unbound Rb (red) and Na (blue) atoms (middle). A pulse of resonant light (blue beam) removes the Na atoms from the lattice (bottom). The remaining Rb atoms are laser cooled (red beam) and the fluorescence photons are collected with an objective, revealing the original positions of the molecules with single-site resolution. **b**, A sample fluorescence image of Rb atoms tagging the positions of molecules in the lattice (left). Molecule occupancy of the lattice for the fluorescence image (right). **c**, Radially averaged density profile of the NaRb molecules (blue) as well as Rb atoms (red) before associating the atoms into molecules. We observe peak fillings of 0.73(2) for the Rb atoms and 0.15(1) for the molecules. Both density profiles are averaged over 30 experimental repetitions. The error bars are standard error of the mean (s.e.m.).

we first study whether intensity interferometry can be used to characterize the distributions of non-interacting Feshbach molecules. We perform an HBT experiment in which we measure the fluctuations in the density distribution of individual clouds of molecules on a grid of detectors after a time of flight (TOF)30. Particles originating from sources A and B can arrive at detectors 1 and 2 in two different ways  $(A \rightarrow 1, B \rightarrow 2 \text{ and } A \rightarrow 2, B \rightarrow 1)$  (Fig. 1). If the two paths are indistinguishable, then their quantum mechanical amplitudes interfere, as reflected in the two-point density correlation function. The correlation relates to the Fourier transform of the source density distribution in the case of a distribution of sources with no phase coherence. As a result, if the positions of the molecules are initially discretized by an optical lattice, the interference pattern exhibits constructive interference peaks whose separation and width are inversely related to the lattice spacing and in situ cloud size, respectively 13,22.

There are two requirements for measuring a high-visibility HBT interference pattern: particle shot-noise-limited detection and a detector spatial resolution better than the interference peak width. To fulfil these conditions, we develop a molecular quantum gas microscope<sup>31–33</sup> to simultaneously prepare and detect over one hundred <sup>23</sup>Na<sup>87</sup>Rb molecules by dissociating them into atoms and using the atoms as tags for the molecule positions.

We form the ultracold bosonic molecules from degenerate gases of Na and Rb atoms by magnetoassociation<sup>34</sup>. To start, dual Na and Rb Bose–Einstein condensates (BECs) are prepared in a single layer of a vertical lattice. Fine adjustment of atom numbers is accomplished using a bichromatic dimple trap, allowing the

reproducible production of clouds of several hundred atoms per species. Both species are prepared in their  $|F=1, m_F=1\rangle$  states, where F and  $m_F$  are the total-angular-momentum quantum number and its projection along the quantization axis, respectively. Next, we make the mixture miscible by nulling the interspecies scattering length using an s-wave Feshbach resonance at 347.6 G (ref. 35). The atoms are then loaded into a two-dimensional (2D) in-plane optical lattice with spacing  $a=752\,\mathrm{nm}$ . The lattice depth is increased to  $36E_{r,Na}$  (where  $E_{r,Na} = h^2/8m_{Na}a^2$  is the recoil energy for Na,  $m_{Na}$  is the atomic mass and h is the Planck constant), crossing the superfluid-to-Mott-insulator transition and freezing tunnelling for both species. We associate the atoms into molecules by adiabatically ramping the magnetic field across the resonance at a rate of 2.5 G ms<sup>-1</sup>, changing the scattering length from attractive to repulsive. For lattice sites containing one atom of each species, the theoretical conversion efficiency is close to unity (Supplementary Section III). We selectively remove the remaining free Na and Rb atoms by transferring them to the  $|2,2\rangle$  hyperfine state and applying resonant light pulses on the optical cycling transitions. The transfer and removal is repeated four times for each species to achieve high efficiency.

To realize a quantum gas microscope for molecules, we employ a three-step process to extract site-resolved positions (Fig. 2a). We first ramp the magnetic field back to the attractive side of the Feshbach resonance, increasing the Franck–Condon overlap between the bound and free states of atoms on a site. We note that a confinement-induced weakly bound state exists here due to the lattice<sup>36</sup>; therefore, an adiabatic ramp across the resonance does not

LETTERS NATURE PHYSICS

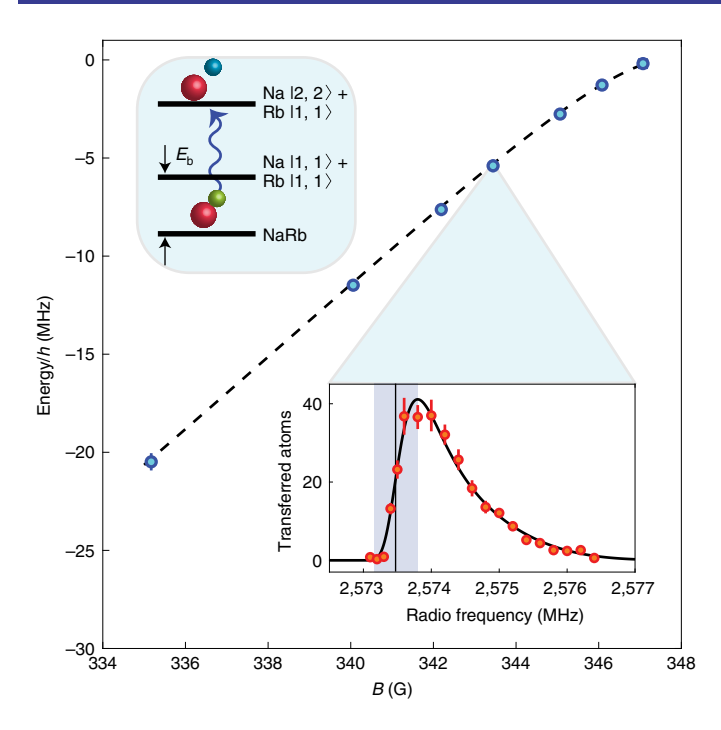


**Fig. 3 | Molecular binding energy versus magnetic field** *B.* For each field, we drive the  $|1,1\rangle\rightarrow|2,2\rangle$  transition in Na to break apart the molecules (upper-left inset) and measure the resulting dissociation spectrum. We extract the bound-free transition frequency from the onset of the spectrum. We also measure the free atomic transition frequency at each field. The difference between the atomic and molecular transition frequencies gives the binding energy (blue circles). The black dashed line is the predicted binding energy from a coupled-channel calculation. The lower-right inset shows an example molecular dissociation spectrum at 343.4 G (red circles) fit to an asymmetric Gaussian (solid black line). The error bars in the inset are the s.e.m. The error on the binding energies is taken as the half-width of the shaded region of the spectrum.

break apart the molecules. The confinement-induced molecules are then dissociated by addressing Na with another series of microwave transfers and optical removal pulses. The remaining Rb atoms serve as markers for the Feshbach molecule locations. Light-assisted collisions during the optical removal pulses are estimated to be negligible (Supplementary Section VI). After ramping the magnetic field to zero, the in-plane lattice depth is increased to  $6,000E_{r,Rb}$  and the atoms are loaded into a light-sheet potential. Optical molasses beams both cool the Rb atoms and scatter photons, which are collected with a high-numerical-aperture objective and imaged onto a camera. The full-width at half-maximum of the point spread function is 1,010(15) nm, which is sufficient for single-site resolution using a reconstruction algorithm<sup>33</sup>.

Figure 2b shows an example image of an in situ cloud of 103 molecules. A radially averaged density profile, averaged over 30 experimental repetitions, is shown in Fig. 2c. We measure a central molecule filling of 0.15(1), compared with the Rb parity-projected central filling of 0.73(2) (Supplementary Section III). The molecule filling fraction can be increased in future work by improving the overlap between the atomic clouds, lowering their temperature and increasing the vertical confinement to obtain stronger interactions at the superfluid-to-Mott-insulator transition.

A high molecule detection fidelity is essential for obtaining high-contrast HBT interference as well as for future applications of molecule microscopy. Possible limitations on the molecule detection fidelity include imperfect atom tagging of sites that had molecules as well as site-to-site hopping and loss of the Rb-tag atoms during

fluorescence imaging. We first measure the false-negative molecule detection rate due to imperfect tagging. After performing the tagging protocol consisting of dissociating the molecules and optically removing Na, we ramp the field to the repulsive side of the Feshbach resonance and remove the Rb-tag atoms. The false-negative rate of 1.2(1)% is obtained by repeating the tagging protocol before fluorescence imaging to identify failures from the first attempt. During our 0.5 s imaging exposure time, we measure site-to-site hopping of 0.1(1)% and 1.7(3)% loss. The latter is consistent with the measured atom lifetime limited by background gas collisions. We additionally measure a false-positive rate of 0.34(5)% due to Rb atoms that did not associate into molecules and were not removed before imaging (Supplementary Section V).

We further confirm that the detected particles are molecules by measuring their binding energy as a function of magnetic field using dissociation spectroscopy (Fig. 3). Driving the  $|1,1\rangle\rightarrow|2,2\rangle$  transition in Na yields the molecular dissociation spectrum, showing a sharp onset at a microwave frequency shifted by binding energy  $E_{\rm b}$  from the atomic transition. Molecules that are not dissociated are not detected in fluorescence imaging. We find close agreement between our measured binding energies and a coupled-channel calculation using the BOUND package<sup>37</sup> based on the parameters mentioned elsewhere<sup>38</sup>. Confinement effects are ignored since they are smaller than the resolution of the measurement.

Having established our molecule detection procedure, we now observe the HBT effect by measuring the density–density correlation function  $g^{(2)}(\mathbf{d})$  after a TOF (Fig. 4). The correlation function is defined as

$$g^{(2)}(\mathbf{d}) = \frac{\int \langle \hat{n}(\mathbf{x})\hat{n}(\mathbf{x}+\mathbf{d})\rangle d^2\mathbf{x}}{\int \langle \hat{n}(\mathbf{x})\rangle \langle \hat{n}(\mathbf{x}+\mathbf{d})\rangle d^2\mathbf{x}},$$
(1)

where  $\hat{n}(\mathbf{x})$  is the number operator at detection position  $\mathbf{x}$ , and  $\mathbf{d}$  is the displacement between the detection positions. Maximal particle bunching is indicated by  $g^{(2)} = 2$ , whereas for uncorrelated particles,  $g^{(2)} = 1$ . For a Gaussian source cloud of half-width s (at  $e^{-1/2}$  of the maximum), the half-width of the interference peaks is given by  $\delta = \hbar t / m s$  (at  $e^{-1}$  of the maximum), where m is the particle mass, t is the TOF and  $\hbar$  is the reduced Planck constant. Although particle shot-noise-limited imaging in a 2D plane can theoretically achieve peak correlation amplitudes of  $g^{(2)} = 2$ , the amplitude reduces if the width of the peaks is narrower than the detector size (in our case, one lattice site). Therefore, we carefully choose our source cloud size and use the largest possible TOF, given the constraints from the size of the lattice beams, to maximize the HBT amplitude.

A larger signal-to-noise ratio of the interference pattern can be achieved for higher in situ lattice filling fractions. Since we achieve higher fillings with atoms than with molecules, we first benchmark the interferometry protocol with Rb atoms. We prepare a gas with 189(20) Rb atoms frozen in a 2D optical lattice (depth,  $66E_{\rm r,Rb}$ ), with peak filling of 0.86(2) and an average source size s=7(1) sites. We abruptly turn off the 2D lattice to initiate a 9.4(1) ms TOF in the vertical lattice. The vertical lattice confinement is set to  $\omega_{\rm Rb}=2\pi\times(3,4,1,000)$  Hz, providing negligible radial confinement. The TOF satisfies the far-field detection condition  $t\gg 2\pi/\omega_{\rm p}$ , where  $\omega_{\rm r}=2\pi\times14\,{\rm kHz}$  is the on-site radial trap frequency of the 2D lattice for Rb (ref.  $^{39}$ ). Following the TOF, we turn on the 2D lattice to pin the distribution for imaging.

The observed atomic HBT correlations are shown in Fig. 4c. We observe a high-contrast interference pattern with average correlation peak amplitudes of 1.80(12) and an average background value of 0.999(6). The measured peak separation and width from the one-dimensional (1D) cut (Fig. 4d) is 75.9(4) and 2.4(2) sites, respectively, close to the theoretically expected spacing of  $ht/m_{\rm Rb}a = 76.2(8)$  and  $\delta = 1.7(3)$  sites. The recapture of the atoms in the 2D pinning lattice may contribute to the observed broadening

NATURE PHYSICS LETTERS

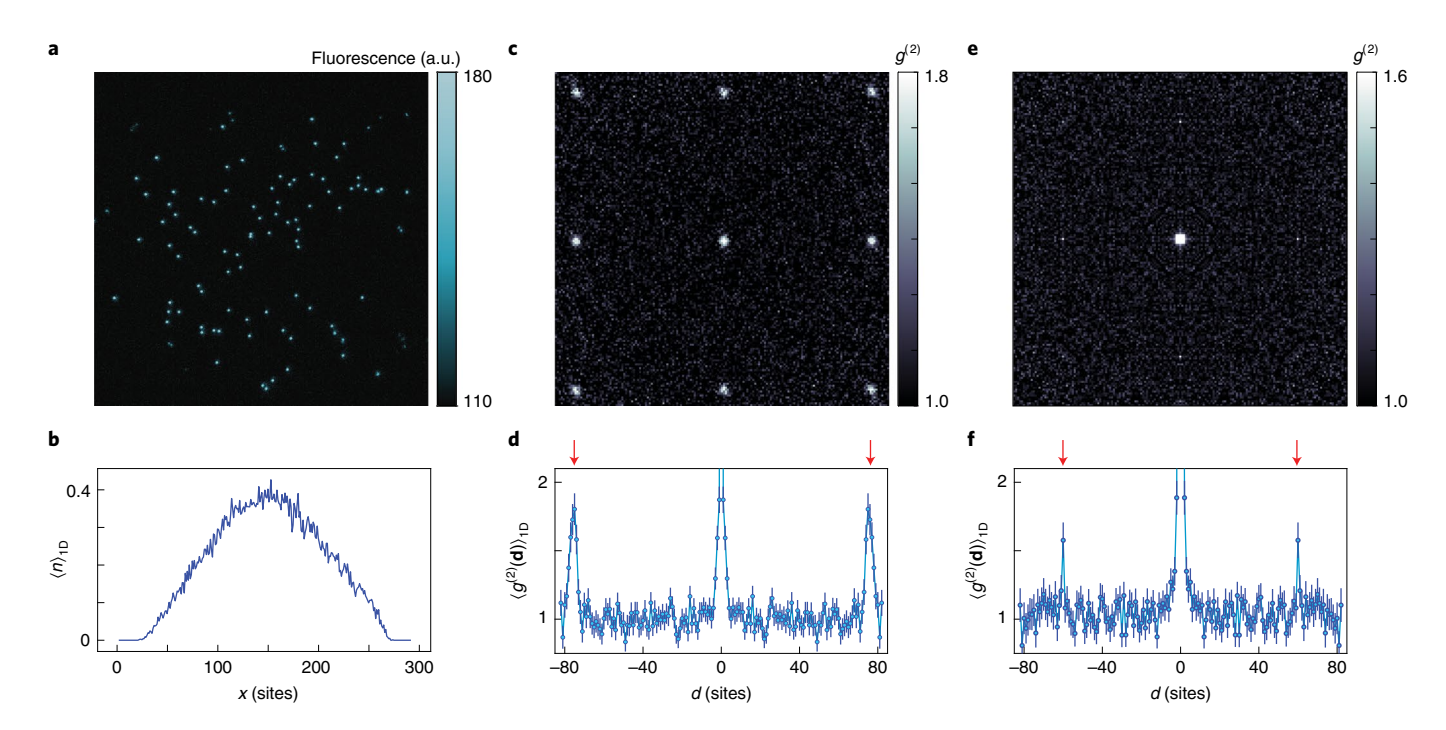


**Fig. 4 | Observation of the HBT effect with molecules. a**, Typical fluorescence image obtained after molecule TOF. **b**, Integrated density profile after TOF, averaged over 764 images. **c**, HBT correlations for Rb atoms, post-selected for images that yielded between 130 and 300 atoms. **d**, Profile of the Rb HBT correlations, taken as the average of 1D cuts along the horizontal and vertical axes of the 2D correlations. The red arrows indicate the predicted position of the interference peaks, corresponding to the reciprocal lattice spacing. **e**, HBT correlations for molecules averaged across the lattice symmetries. Images with fewer than 20 molecules were excluded from the analysis. **f**, Profile of the NaRb HBT correlations, taken as the average of 1D cuts along the horizontal and vertical axes of the 2D correlations. The red arrows indicate the predicted position of the interference peaks. The error bars are the s.e.m.

of the peak width<sup>40</sup>. The symmetric pattern verifies that the 2D lattice axes are orthogonal and the lattice spacings along both axes are identical to better than 0.5%. This implies that  $g^{(2)}(\mathbf{d})$  is invariant for  $\mathbf{d}$  reflected across the x=0, y=0, x=y and x=-y symmetry axes, justifying the averaging of the weaker molecular correlations across the lattice symmetries to reduce noise.

We repeat the HBT interferometry with 56(13) molecules and a mean source size  $s \approx 17$  sites, which is expected to produce interference peaks whose widths are of the order of the lattice spacing. The protocol is the same as that used for atoms, with molecules released from the 2D lattice at a magnetic field of 335.1 G (with binding energy  $E_b/h \approx 20 \,\mathrm{MHz}$ ). Figure 4e,f shows the observed molecular correlations averaged across the lattice symmetries. Since the TOF is the same as that used in the Rb-atom correlation measurement, the smaller correlation peak spacing for the molecules is a direct result of their increased mass. The measured spacing is 60.0(5) sites, consistent with the theoretical expectation of 60.3(6) sites. Although the correlation peaks are narrower than for Rb (<1 site), the peak amplitude remains large at 1.58(13). The average baseline is 1.04(1), with the deviation from unity caused by correlations at all distances due to shot-to-shot molecule number fluctuations. The interference contrast is sensitive to the preparation of the molecules in the same internal state and the same motional state of the vertical lattice, since these quantum numbers can provide which-path information during the free expansion; therefore, the measured contrast of 0.54(13) indicates a high degree of indistinguishability of the molecules (Supplementary Section IX).

To conclude, we have demonstrated site-resolved measurements of density correlation functions in a non-interacting molecular quantum gas after TOF expansion. The observation of the HBT effect with molecules paves the way towards realizing other quantum optical phenomena with molecules of increasing complexity<sup>41</sup>. By transferring the Feshbach molecules to the rovibrational

ground state<sup>1,42</sup>, which has been already demonstrated for NaRb (ref. <sup>43</sup>), a molecular lattice gas with strong dipolar interactions can be prepared. The interplay of quantum statistics and interactions can give rise to interesting signatures in HBT measurements<sup>20,21</sup>. In addition, many correlated quantum states predicted to be realizable with polar molecules also exhibit real-space density correlations that can be directly measured with a molecule microscope, including Wigner crystals<sup>44</sup> and Mott solids with rational lattice fillings<sup>45</sup>. Finally, by encoding a pseudospin using a rotational degree of freedom, the microscope can be used to study spin correlations in quantum magnets<sup>29</sup>.

# Online content

Any methods, additional references, Nature Research reporting summaries, source data, extended data, supplementary information, acknowledgements, peer review information; details of author contributions and competing interests; and statements of data and code availability are available at https://doi.org/10.1038/s41567-022-01695-9.

Received: 22 November 2021; Accepted: 27 June 2022; Published online: 11 August 2022

# References

- Bohn, J. L., Rey, A. M. & Ye, J. Cold molecules: progress in quantum engineering of chemistry and quantum matter. Science 357, 1002–1010 (2017).
- DeMille, D. Quantum computation with trapped polar molecules. Phys. Rev. Lett. 88, 067901 (2002).
- 3. Brown, R. H. & Twiss, R. Q. A new type of interferometer for use in radio astronomy. *Philos. Mag.* 45, 663–682 (1954).
- Brown, R. H. & Twiss, R. Q. Correlation between photons in two coherent beams of light. *Nature* 177, 27–29 (1956).
- Glauber, R. J. The quantum theory of optical coherence. Phys. Rev. 130, 2529 (1963).

LETTERS NATURE PHYSICS

- Baym, G. The physics of Hanbury Brown–Twiss intensity interferometry: from stars to nuclear collisions. Acta Phys. Pol. B 29, 1839–1884 (1998).
- 7. Henny, M. et al. The fermionic Hanbury Brown and Twiss experiment. *Science* **284**, 296–298 (1999).
- Oliver, W. D., Kim, J., Liu, R. C. & Yamamoto, Y. Hanbury Brown and Twiss-type experiment with electrons. Science 284, 299–301 (1999).
- Iannuzzi, M., Orecchini, A., Sacchetti, F., Facchi, P. & Pascazio, S. Direct experimental evidence of free-fermion antibunching. *Phys. Rev. Lett.* 96, 080402 (2006).
- Cohen, J. D. et al. Phonon counting and intensity interferometry of a nanomechanical resonator. *Nature* 520, 522–525 (2015).
- 11. Riedinger, R. et al. Non-classical correlations between single photons and phonons from a mechanical oscillator. *Nature* **530**, 313–316 (2016).
- Yasuda, M. & Shimizu, F. Observation of two-atom correlation of an ultracold neon atomic beam. *Phys. Rev. Lett.* 77, 3090 (1996).
- Fölling, S. et al. Spatial quantum noise interferometry in expanding ultracold atom clouds. *Nature* 434, 481–484 (2005).
- Öttl, A., Ritter, S., Köhl, M. & Esslinger, T. Correlations and counting statistics of an atom laser. *Phys. Rev. Lett.* 95, 090404 (2005).
- Schellekens, M. et al. Hanbury Brown Twiss effect for ultracold quantum gases. Science 310, 648–651 (2005).
- Jeltes, T. et al. Comparison of the Hanbury Brown–Twiss effect for bosons and fermions. Nature 445, 402–405 (2007).
- Hodgman, S., Dall, R., Manning, A., Baldwin, K. & Truscott, A. Direct measurement of long-range third-order coherence in Bose-Einstein condensates. *Science* 331, 1046–1049 (2011).
- Perrin, A. et al. Hanbury Brown and Twiss correlations across the Bose– Einstein condensation threshold. Nat. Phys. 8, 195–198 (2012).
- 19. Dall, R. et al. Ideal *n*-body correlations with massive particles. *Nat. Phys.* **9**, 341–344 (2013).
- Carcy, C. et al. Momentum-space atom correlations in a Mott insulator. *Phys. Rev. X* 9, 041028 (2019).
- Tenart, A., Hercé, G., Bureik, J.-P., Dareau, A. & Clément, D. Observation of pairs of atoms at opposite momenta in an equilibrium interacting Bose gas. Nat. Phys. 17, 1364–1368 (2021).
- 22. Rom, T. et al. Free fermion antibunching in a degenerate atomic Fermi gas released from an optical lattice. *Nature* **444**, 733–736 (2006).
- Preiss, P. M. et al. High-contrast interference of ultracold fermions. Phys. Rev. Lett. 122, 143602 (2019).
- Köhler, T., Góral, K. & Julienne, P. S. Production of cold molecules via magnetically tunable Feshbach resonances. *Rev. Mod. Phys.* 78, 1311–1361 (2006).
- 25. Tarbutt, M. R. Laser cooling of molecules. Contemp. Phys. 59, 356-376 (2018).
- 26. Anderegg, L. et al. An optical tweezer array of ultracold molecules. *Science* **365**, 1156–1158 (2019).
- Zhang, J. T. et al. Forming a single molecule by magnetoassociation in an optical tweezer. *Phys. Rev. Lett.* 124, 253401 (2020).
- 28. He, X. et al. Coherently forming a single molecule in an optical trap. *Science* **370**, 331–335 (2020).

- 29. Yan, B. et al. Observation of dipolar spin-exchange interactions with lattice-confined polar molecules. *Nature* **501**, 521–525 (2013).
- Altman, E., Demler, E. & Lukin, M. D. Probing many-body states of ultracold atoms via noise correlations. *Phys. Rev. A* 70, 013603 (2004).
- 31. Bakr, W. S. et al. Probing the superfluid-to-Mott insulator transition at the single-atom level. *Science* **329**, 547–550 (2010).
- Sherson, J. F. et al. Single-atom-resolved fluorescence imaging of an atomic Mott insulator. *Nature* 467, 68–72 (2010).
- 33. Gross, C. & Bakr, W. S. Quantum gas microscopy for single atom and spin detection. *Nat. Phys.* 17, 1316–1323 (2021).
- Wang, F. et al. Formation of ultracold NaRb Feshbach molecules. New J. Phys. 17, 035003 (2015).
- Wang, F., Li, X., Xiong, D. & Wang, D. A double species <sup>23</sup>Na and <sup>87</sup>Rb Bose–Einstein condensate with tunable miscibility via an interspecies Feshbach resonance. *J. Phys. B* 49, 015302 (2015).
- Stöferle, T., Moritz, H., Günter, K., Köhl, M. & Esslinger, T. Molecules of fermionic atoms in an optical lattice. *Phys. Rev. Lett.* 96, 030401 (2006).
- Hutson, J. M. & Le Sueur, C. R. BOUND and FIELD: programs for calculating bound states of interacting pairs of atoms and molecules. *Comput. Phys. Commun.* 241, 1–8 (2019).
- 38. Guo, Z. et al. Improved characterization of Feshbach resonances and interaction potentials between <sup>23</sup>Na and <sup>87</sup>Rb atoms. *Phys. Rev. A* 105, 023313 (2022).
- 39. Fölling, S. Quantum noise correlation experiments with ultracold atoms. in *Quantum Gas Experiments* 145–177 (World Scientific, 2014).
- Pyzh, M., Krönke, S., Weitenberg, C. & Schmelcher, P. Quantum point spread function for imaging trapped few-body systems with a quantum gas microscope. New J. Phys. 21, 053013 (2019).
- 41. Mitra, D. et al. Direct laser cooling of a symmetric top molecule. *Science* **369**, 1366–1369 (2020).
- Ni, K.-K. et al. A high phase-space-density gas of polar molecules. Science 322, 231–235 (2008).
- Guo, M. et al. Creation of an ultracold gas of ground-state dipolar <sup>23</sup>Na<sup>87</sup>Rb molecules. *Phys. Rev. Lett.* 116, 205303 (2016).
- Büchler, H. P. et al. Strongly correlated 2D quantum phases with cold polar molecules: controlling the shape of the interaction potential. *Phys. Rev. Lett.* 98, 060404 (2007).
- Capogrosso-Sansone, B., Trefzger, C., Lewenstein, M., Zoller, P. & Pupillo, G. Quantum phases of cold polar molecules in 2D optical lattices. *Phys. Rev. Lett.* 104, 125301 (2010).

**Publisher's note** Springer Nature remains neutral with regard to jurisdictional claims in published maps and institutional affiliations.

Springer Nature or its licensor holds exclusive rights to this article under a publishing agreement with the author(s) or other rightsholder(s); author self-archiving of the accepted manuscript version of this article is solely governed by the terms of such publishing agreement and applicable law.

© The Author(s), under exclusive licence to Springer Nature Limited 2022

NATURE PHYSICS LETTERS

### Methods

Here we describe the formation of ultracold bosonic <sup>23</sup>Na<sup>87</sup>Rb molecules by magnetoassociation from degenerate gases of Na and Rb atoms. NaRb molecules have been produced in bulk mixtures elsewhere<sup>34</sup>.

We start by creating dual Na/Rb BECs with typically 2×105 atoms of each species in the  $|F=1, m_F=-1\rangle$  state, using Na as a sympathetic coolant for Rb during forced evaporative cooling in a quadrupole magnetic trap followed by evaporation in a crossed 1,064 nm optical dipole trap. To prepare a 2D system, we load the condensates into a 1,064 nm light sheet with tight confinement along the vertical direction ( $\omega_{\text{Na}} = 2\pi \times (24, 117, 1,900)$  Hz,  $\omega_{\text{Rb}} = 0.86\omega_{\text{Na}}$ ). We then transfer both atom species to the  $|F=1, m_F=1\rangle$  state, the entrance channel for the relevant Feshbach resonance. To further increase the vertical confinement, the atoms are loaded into a single layer of a 3.8- $\mu m\text{-spacing}$  vertical lattice created by two  $1,\!064\,nm$  beams intersecting at 16° ( $\omega_{Na} = 2\pi \times (14, 20, 4,500)$  Hz). For our optical lattice approach of molecule formation, we need the central density of the clouds to be of the order of one atom per site for each species. Given our trap parameters, this requires the ability to reproducibly generate small condensates of the order of one hundred atoms. We achieve this by performing a second stage of evaporative cooling in a tightly focused bichromatic dimple trap, which allows for independent adjustment of the atom number in each species (Supplementary Section II).

At a near-zero magnetic field, Na and Rb BECs are immiscible. To increase the overlap of the spatial distributions before magnetoassociation, we tune the interspecies scattering length using an s-wave Feshbach resonance at 347.6 G to bring the clouds into the miscible regime<sup>35</sup>. We quickly ramp the field above resonance to 415.9 G and then slowly decrease the field to the zero crossing of the interspecies scattering length at 351.9 G in 20 ms. We subsequently load the 2D mixture into an in-plane square lattice with spacing a = 752 nm created by the fourfold interference of a single  $1,064\,\mathrm{nm}$  beam ( $105\,\mathrm{\mu m}$  waist) in a bowtie configuration<sup>46</sup>. We freeze tunnelling for both species by ramping the in-plane lattice depth to  $36E_{r,Na}$ , where  $E_{r,Na} = h^2/8m_{Na}a^2$  is the recoil energy for Na. Next, we ramp the magnetic field below resonance at a rate of 2.5 G ms<sup>-1</sup> to form Feshbach molecules. For lattice sites containing one atom of each species, the theoretical conversion efficiency is very close to unity (Supplementary Section III). We selectively remove the remaining free atoms by transferring them to  $|2,2\rangle$  with a microwave Landau-Zener sweep at a field of ~346.6 G (molecular binding energy  $E_b/h \approx 0.7 \,\text{MHz}$ ) and applying resonant light on the  $|2,2\rangle$  to  $|3,3\rangle$  optical cycling transition. The transfer and removal is repeated four times for each species to achieve high efficiency, as described earlier.

For imaging, the magnetic field is brought to 0 G, the in-plane lattice depth is increased to  $6,000E_{c,Rb}$  and the Rb atoms are loaded back into the light sheet

at a depth of  $140\,\mu K$ . Optical-molasses cooling light scatters photons into a 0.5-numerical-aperture objective, with  $\sim\!10^4\,photons$  collected on the camera per atom per second.

### Data availability

Source data can be found in the Harvard Dataverse  $^{47}$ . All other supporting data are available from the corresponding author upon reasonable request.

### References

- Sebby-Strabley, J., Anderlini, M., Jessen, P. S. & Porto, J. V. Lattice of double wells for manipulating pairs of cold atoms. *Phys. Rev. A* 73, 033605 (2006).
- Rosenberg, J., Christakis, L., Guardado-Sanchez, E., Yan, Z. & Bakr, W. Replication data for: observation of the Hanbury Brown and Twiss effect with ultracold molecules. *Harvard Dataverse* https://doi.org/10.7910/DVN/ QTROX3 (2022).

### Acknowledgements

We would like to thank G. Zheng, S. Aggarwal, A. Morningstar and R. Raj for experimental assistance. This work was supported by the NSF (grant no. 1912154) and the David and Lucile Packard Foundation (grant no. 2016-65128). L.C. was supported by the NSF Graduate Research Fellowship Program.

## **Author contributions**

W.S.B. conceived the study and supervised the experiment. J.S.R., L.C., E.G.-S. and Z.Z.Y performed the experiments. J.S.R., L.C. and Z.Z.Y performed the data analysis. All the authors contributed to the article.

### **Competing interests**

The authors declare no competing interests.

### Additional information

**Supplementary information** The online version contains supplementary material available at https://doi.org/10.1038/s41567-022-01695-9.

Correspondence and requests for materials should be addressed to Waseem S. Bakr.

**Peer review information** *Nature Physics* thanks Hanns-Christoph Nägerl and the other, anonymous, reviewer(s) for their contribution to the peer review of this work.

Reprints and permissions information is available at www.nature.com/reprints.